Citation for final published version:

Eblabla, A., Li, X., Alathbah, M., Wu, Z., Lees, J. and Elgaid, K. 2019. Multi-channel AlGaN/GaN lateral schottky barrier diodes on low-resistivity silicon for sub-THz integrated circuits applications. IEEE Electron Device Letters 40 (6) , pp. 878-880. 10.1109/LED.2019.2912910 file

Publishers page: http://dx.doi.org/10.1109/LED.2019.2912910
<http://dx.doi.org/10.1109/LED.2019.2912910>

# Multi-channel AlGaN/GaN Lateral Schottky Barrier Diodes on Low Resistivity Silicon for Sub-THz Integrated Circuits Applications

A. Eblabla, X. Li, M. Alathbah, Z. Wu, J. Lees and K. Elgaid

***Abstract*— This work presents novel multi-channel RF lateral Schottky-barrier diodes (SBDs) based on AlGaN/GaN on Low Resistivity (LR) ($\sigma = 0.02$ Ω.cm) silicon substrates. The developed technology offers a reduction of 37 % in onset voltage, $V_{ON}$ (from 1.34 to 0.84 V), and 36 % in ON-resistance, $R_{ON}$ (1.52 to 0.97 to Ω.mm) as a result of lowering the Schottky barrier height, $\phi_n$, when compared to conventional lateral SBDs. No compromise in reverse-breakdown voltage and reverse-bias leakage current performance was observed as both multi-channel and conventional technologies exhibited $V_{BV}$ of ($V_{BV} > 30$ V) and $I_R$ of ($I_R < 38$ µA/mm), respectively. Furthermore, a precise small-signal equivalent circuit model was developed and verified for frequencies up to 110 GHz. The fabricated devices exhibited cut-off frequencies of up to 0.6 THz, demonstrating the potential use of lateral AlGaN/GaN SBDs on LR silicon for high-efficiency high-frequency Integrated Circuits applications.**

***Index Terms*— GaN, RF diodes, lateral Schottky barrier diode, sub-THz applications, fin-FET, GaN on silicon.**

## I. INTRODUCTION

Due to the superior electrical properties of III nitride semiconductors, lateral AlGaN/GaN Schottky-barrier diodes (SBDs) grown on LR silicon substrates are emerging as a promising device technology for fast switching speed, high-power, low-cost and compact-size communications and radar applications, such as mixers, frequency multipliers, detectors and tunable filters operating at millimeter wave frequencies [1] [2]. GaN-based SBDs with low onset voltage ($V_{ON}$), high reverse-breakdown ($V_{BV}$) voltage, and low reverse-current leakage ($I_R$), high-switching speed ($R_{ON}$) and high cutoff frequency ($f_c$) are essentially required to compete with current III-V technologies [3]. Conventional GaN-based SBD DC and RF performance is still limited to their large $V_{ON}$, switching loss and RF leakage when utilizing LR Si substrates. Several researchers have recently proposed low $V_{ON}$ along with low $I_R$ and high $V_{BV}$ technologies, including recessed anode, dual-filed plates, regrowth cathodes, and dual- channel field-effect rectifier (LFER) [4] [5] [6]. However, these approaches require accurate control of anode etching to the 2DEG and a complicated fabrication process, which incorporates reliability issues and extra processing cost. Nevertheless, a 3-D SBDs integrated with a tri-gate MOS structure has shown outstanding DC characteristics at the expense of RF performance owing to the inherently large junction capacitance ($C_j$) and series resistance ($R_S$) [7]. Therefore, these techniques are only limited to low-frequency applications. To date, most of the research effort into GaN-based SBDs on silicon is predominantly focused on power electronics, with limited literature targeting RF operation. However, achieving high $f_c$ while maintaining low $I_R$ and superior $V_{BV}$ remains a challenge [1].

In this letter, an optimized multi-channel RF AlGaN/GaN SBDs on LR Si structure is demonstrated using a cost-effective (GaN on LR Si) which is fully compatible with III-V THz monolithic integrated circuit (THz-MIC) technology. In contrast to conventional SBDs, the newly developed devices significantly enhanced the turn-on characteristics, switching loss, ideality factor ($\eta_n$) and $f_C$, where a $V_{ON} = 0.84$ V, $R_{ON} = 0.97$ Ω.mm, $V_{BV} > 30$ V, $\eta_n = 1.69$ and $f_C = 0.6$ THz were achieved. This attributes to the direct contact of Schottky anode to 2DEG at the sidewalls of the multi-mesa trenches along with proper design geometries to suppress substrate coupling effects.

## II. DEVICE DESIGN AND FABRICATION

Fig. 1 indicates a cross-section of the fabricated AlGaN/GaN SBDs on LR Si using a multi-channel structure, which was simultaneously fabricated with conventional SBDs on the same substrate to allow precise comparison. A combination of multi-mesa and T-shaped structures was adopted to form the anode to reduce Schottky barrier height and anode resistivity, respectively. The height ($H_F$), width ($W_F$), spacing ($S_F$) and length ($L_F$) of the nanowires were ~ 50, 41, 89 nm and 2 µm, respectively. The Anode length ($L_A$) and anode head length ($L_{AH}$) were 0.550 µm and 1.1 µm, respectively, whereas the junction length ($L_j$) was 4.28 µm. The total physical anode

Manuscript received January 16, 2019; revised April 6, 2019; accepted April 14, 2019. This work was supported by the Engineering and Physical Sciences Research Council under Grants EP/N014820/2 and EP/P006973/1.

A. Eblabla, M. Alathbah, Z. Wu, J. Lees and K. Elgaid are with the School of Engineering, Cardiff University, Cardiff, CF24 3AA, UK. (email: eblablaa@cardiff.ac.uk).

X. Li is with the School of Engineering, The University of Glasgow, Glasgow, G12 8LT, UK.

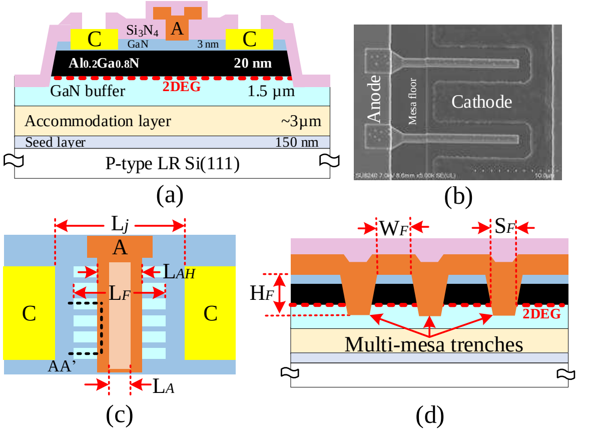

Fig. 1: (a) Cross-sectional view, (b) Scanned-electron microscope (SEM) image and (c) Top-view of the multi-channel SBDs. (d) Cross-sectional representation of the tri-anode along line AA'.

width was 2 × 10 µm, while the effective anode width for the fin-like anode structure was 2 × 5.829 µm.

The epitaxy material used in this work was grown on LR Si (111) (σ = 0.02 Ω.cm) provided by Nexperia. The epilayer consists of 4.65 µm buffer, 20 nm $Al_{0.2}Ga_{0.8}N$ barrier and 3 nm GaN cap layer. A sheet carrier density of 5.9 × $10^{12}$ $cm^{-2}$ and electron mobility of 1713 $cm^2$/Vs are determined using Hall measurements. The device fabrication started with defining the Ti/Pt markers, followed by the deposition of Ti/Al/Ni/Au ohmic contacts and rapid thermal annealing at 790 $^0$C in $N_2$ environment to form the cathode. Next, a ~150 nm depth mesa isolation was performed through $Cl_2$/Ar-based inductively-coupled plasma (ICP). Then, multi-mesa trenches were defined by e-beam lithography and subsequently etched using $Cl_2$/Ar-based ICP with an etch depth of ~ 50 nm. A 100 nm $Si_3N_4$ passivation layer was then deposited using a low-stress inductively-coupled plasma chemical vapour deposition (ICP-CVD) at room temperature. To form the T-shaped anode, E-beam lithography was used to define anode-foot trenches through the $Si_3N_4$ passivation layer using a low-damage $SF_6$/$N_2$ gas mixture reactive-ion etching (RIE), which was followed by Ni/Au metal stack evaporation to finish the T-shaped anode. Windows in the $Si_3N_4$ at the cathode areas were etched prior to the deposition of Ti/Au bond pads and 160 nm $Si_3N_4$ layer as a final passivation layer. Device fabrication was finalized by $Si_3N_4$ etching in the measurement pad regions. SEM image of the fabricated devices in shown in Fig.1b.

## III. RESULTS AND DISCUSSION

### A. *DC Characteristics*

Fig. 2 indicates the typical *I-V* characteristics of the fabricated conventional and multi-channel structures at room temperature using both linear and logarithm scales. The diode current (A/mm) and resistance (Ω.mm) of conventional and multi-channel structures are normalized by the total physical anode width (2 × 10 µm) and effective anode width (2 × 5.829 µm), respectively. Fig. 2a reveals that incorporating a multi-channel anode structure reduced $V_{ON}$ from 1.34 to 0.84 V together with improved $R_{ON}$ from 1.52 to 0.97 to Ω.mm. This attributes to the direct anode contact to the 2DEG, where the anode is wrapped around the narrow AlGaN/GaN bodies.

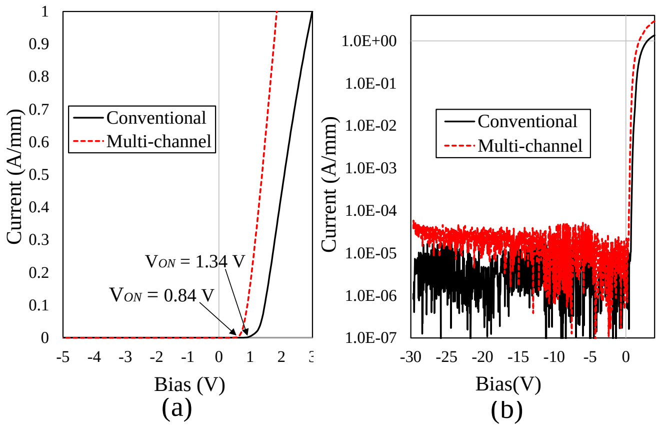

Fig. 2: *I-V* characteristics of a fabricated SBD plotted in (a) Linear and (b) Logarithm scale.

To further analyze these findings, the semilog *I-V* plot (shown in Fig. 2b) is used, which allows the extraction of $\eta_n$ and $\phi_{n.}$ based on the analytical equations indicated in [8]. Both device structures exhibited $\eta_n$ between 1 and 2, which indicates the presence of conduction mechanism besides a thermionic emission mechanism [9]. An improvement of 14.28 % in $\eta_n$ (from 1.97 to 1.69) was obtained by the developed multi-channel structure as compared to conventional SBDs. Furthermore, the observed reduction in $V_{ON}$ when using the new structure corresponds to a reduction of 17.5 % in $\phi_n$ (from 0.78 to 0.64 eV). However, $I_R$ was slightly increased with the multi-channel structure, where $I_R$ < 38 µA/mm was performed at a reverse voltage of up to 30 V. This attributes to the additional anode length where the anode is in direct contact to the GaN buffer in the multi-mesa floor regions. The achieved results are comparable to that of SBDs on semi-insulating (SI)-SiC with recessed anode and regrowth cathode technologies, with better $V_{BV}$ and $I_R$ [1]. This enhancement is mainly attributed to the scale of anode-to-cathode spacing and the use of T-shaped anode, owing to the reduction in peak electric field of Schottky junction [5].

### B. *RF Characteristics*

On-wafer small-signal *S*-parameters measurements were performed in the frequency range 0.1 to 110 GHz using an Agilent PNA network analyzer (E8361A) and frequency extenders (N5260A). The system was calibrated with an off-wafer calibration impedance standard substrate (ISS), using a Short-Open-Load-Thru (SOLT) calibration technique.

Fig. 3a shows the extracted small-signal circuit model of the devices, which was validated by the good agreement between modelled and measured *S*-parameters up to 110 GHz, as shown in Fig. 3b. This allows the extraction of SBD intrinsic elements; junction resistance ($R_j$), $C_j$ and $R_s$, which used to determine $f_c$ of the fabricated devices. As indicated in Fig. 3a, unlike SI-substrates, substrate parasitics ($S_{sub}$ and $R_{sub}$) are incorporated into the standard SBD circuit model when considering lossy Si

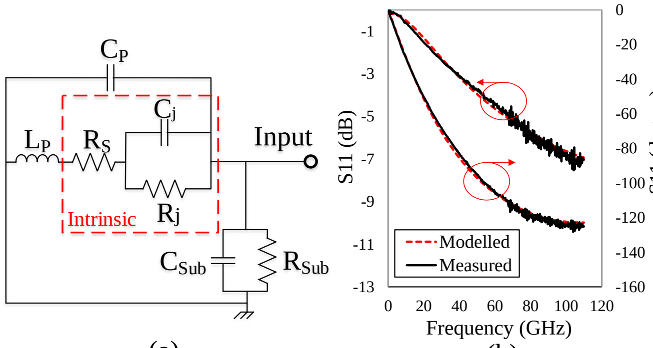

(a) (b)

Fig. 3: (a) Schematic of the proposed small-signal equivalent circuit model and (b) measured versus modelled *S*-parameters of the fabricated multi-channel AlGaN\GaN SBDs on LR Si at 0 V bias.

Table I
EXTRACTED PARAMETERS FOR THE EQUIVALENT CIRCUIT MODEL FOR THE FABRICATED LATERAL SBDs AT 0 V BIAS.

| SBD structure | Intrinsic | | | *Extrinsic* | | | |
|---|---|---|---|---|---|---|---|
| | ***$C_j$* (fF)** | ***$R_s$* (Ω)** | ***$R_j$* (KΩ)** | ***$L_p$* (pH)** | ***$C_p$* (fF)** | ***$C_{sub}$* (fF)** | ***$R_{sub}$* (KΩ)** |
| Conventional | 49.1 | 44.9 | 11.6 | 40.3 | 26.4 | 3.1 | 10.3 |
| Multi-channel | 46.4 | 51.9 | 11.6 | | | | |

as a substrate. Furthermore, $C_p$ and $L_P$ represents pad parasitics. However, the external parasitic elements have a significant influence on the model at frequencies beyond 20 GHz.

Table I shows the extracted circuit element values of conventional and multi-channel structures at 0 V bias. In contrast to conventional SBDs, an increase in $R_S$ by 15.6 % (44.9 to 51.9 Ω) and a slight reduction in $C_j$ by 5.5 % (form 49.1 to 46.4 fF) were observed for the newly developed fin-type technology. This attributes to the additional anode length in the multi-mesa trenches and reduction in $\phi_n$, respectively. In addition, the low value of $C_{sub}$ and high value of $R_{sub}$ indicates that substrate coupling effect could be neglected in both design structures. This was a result of the proper design geometries where the anode-to-cathode separation (2.415 µm) is less than the buffer thickness (4.65 µm) [10].

The extracted values of $C_j$ as a function of the applied voltage of the fabricated devices are shown in Fig. 4a. It can be seen that $C_j$ was inversely proportional to the applied reverse voltage, where a sharp drop in $C_j$ was obtained when changing the voltage form 0 to -2 V. Furthermore, owing to the direct anode contact to 2DEG for multi-channel SBDs, $C_j$ was significantly reduced at reverse biases beyond -2 V, as compared to conventional SBDs. This reflected a dramatic enhancement in $f_C$ which can be calculated from $R_s$ and $C_j$ [1]. Therefore, $f_C$ was improved by 32.7 % (from 0.457 to 0.607 THz), as shown in Fig. 4.b. However, the achieved $f_C$ of the fabricated lateral SBDs on LR Si is still limited to their larger $R_S$, which mainly depends on material growth quality and cathode contact resistivity, as compared to SBDs realized on GaN-on-SI-SiC substrates [1].

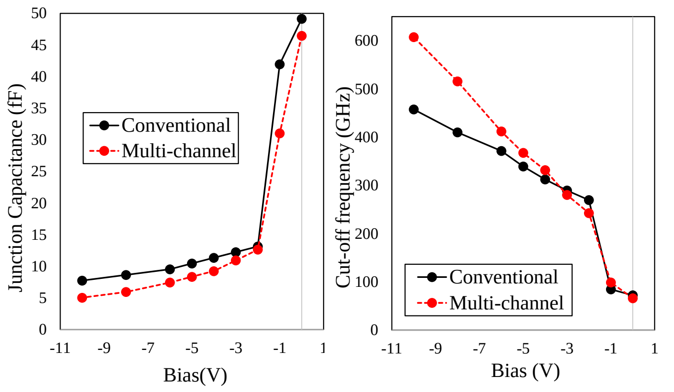

(a) (b)

Fig. 4: Junction capacitance ($C_j$) versus voltage, and (b) Cut-off frequency ($f_C$) versus voltage of the fabricated conventional and multi-channel SBDs.

## IV. CONCLUSION

A newly developed multi-channel RF lateral AlGaN/GaN SBD on LR Si technology has been realized in this work. A $V_{ON}$ of 0.84 V along with $R_{ON}$ of 0.97 Ω.mm and $\eta_n$ of 1.69 were achieved as a result of the direct Schottky anode contact to the 2DEG resulting in a $\phi_n$ of 0.64 eV. The fabricated devices exhibited $V_{BV}$ of greater than 30 V along with $I_R$ of less than 38 µm/mm. In addition, a newly proposed small-signal circuit model was introduced up to 110 GHz. An $f_c$ of 0.6 THz at a reverse bias of -10 V was achieved as a result of the optimized SBD design structure and geometries. These findings enable an effective pathway for the realization of high-performance sub-THz-MIC topologies.

## V. REFERENCES

[1] K. Shinohara, D. C. Regan, Y. Tang, A. L. Corrion, D. F. Brown, J. C. Wong, J. F. Robinson, H. H. Fung, A. Schmitz, T. C. Oh, S. J. Kim, P. S. Chen, R. G. Nagele, A. D. Margomenos, and M. Micovic, "Scaling of GaN HEMTs and Schottky Diodes for Submillimeter-Wave MMIC Applications," in *IEEE Transactions on Electron Devices*, vol. 60, no. 10, pp. 2982-2996, Oct. 2013. DOI: 10.1109/TED.2013.2268160.

[2] T. Boles and G. Lopes, "GaN Schottky diodes for RF wireless power detection and conversion," *2015 European Microwave Conference (EuMC)*, Paris, 2015, pp. 1003-1006. DOI: 10.1109/EuMC.2015.7345935.

[3] B. Ren, M. Liao, M. Sumiya, L. Wang, Y. Koide, and L. Sang, "Nearly ideal vertical GaN Schottky barrier diodes with ultralow turn-on voltage and on-resistance," in *Applied Physics Express*, vol. 10, no. 5, pp. 051001, March 2017.DOI: 10-7567/APEX.10.051001.

[4] Y. Lian, Y. Lin, J. Yang, C. Cheng and S. S. H. Hsu, "AlGaN/GaN Schottky Barrier Diodes on Silicon Substrates With Selective Si Diffusion for Low Onset Voltage and High Reverse Blocking," in *IEEE Electron Device Letters*, vol. 34, no. 8, pp. 981-983, Aug. 2013. DOI: 10.1109/LED.2013.2269475.

[5] M. Zhu, B. Song, M. Qi, Z. Hu, K. Nomoto, X. Yan, Y. Cao, W. Johnson, E. Kohn, D. Jena, and H. G. Xing, "1.9-kV AlGaN/GaN Lateral Schottky Barrier Diodes on Silicon," in *IEEE Electron Device Letters*, vol. 36, no. 4, pp. 375-377, April 2015. DOI: 10.1109/LED.2015.2404309.

[6] J. Gao, M. Wang, R. Yin, S. Liu, C. P. Wen , J. Wang, W. Wu, Y. Hao, Y. Jin, and B. Shen, "Schottky-MOS Hybrid Anode AlGaN/GaN Lateral Field-Effect Rectifier With Low Onset Voltage and Improved Breakdown Voltage," in *IEEE Electron Device Letters*, vol. 38, no. 10, pp. 1425-1428, Oct. 2017. DOI: 10.1109/LED.2017.2737520.

[7] J. Ma and E. Matioli, "High-Voltage and Low-Leakage AlGaN/GaN Tri-Anode Schottky Diodes With Integrated Tri-Gate Transistors," in *IEEE Electron Device Letters*, vol. 38, no. 1, pp. 83-86, Jan. 2017. DOI:

10.1109/LED.2016.2632044

[8] M. Rudan, *Physics of Semiconductor Devices*, 2nd Ed., Springer International Publishing, 2018. DOI: 10.1007/978-3-319-63154-7.

[9] B.-S. Wang, G.-Y. Lee, C.-C. Yang, I. Sanyal, and J.-I. Chyi, “Enhancing the Performance of AlGaN/GaN Schottky Barrier Diodes by $SF_6$ Plasma Treatment and Deep Anode Recess,” in *ECS Journal of Solid State Science and Technology*, vol. 6, no. 11, pp. S3081–S3083, Sept. 2017. DOI: 10.1149/2.0081711jss.

[10] A. Eblabla, X. Li, I. Thayne, D. J. Wallis, I. Guiney and K. Elgaid, "High Performance GaN High Electron Mobility Transistors on Low Resistivity Silicon for X-Band Applications," in *IEEE Electron Device Letters*, vol. 36, no. 9, pp. 899-901, Sept. 2015. DOI: 10.1109/LED.2015.2460120.